Optics Letters

Quickly tunable ultra-narrow filter via a metal film waveguide

Hongrui Shan,[1,†] Qiheng Wei,[1,†] Hailang Dai,[1,3] and Xianfeng Chen[1,2,*]

[1] State Key Laboratory of Advanced Optical Communication Systems and Networks, School of Physics and Astronomy, Shanghai Jiao Tong University, Shanghai 200240, China

[2] Collaborative Innovation Center of Light Manipulations and Applications, Shandong Normal University, Jinan 250358, China

[3] hailangdai@sjtu.edu.cn

[†] These authors contributed equally to this Letter.

*xfchen@sjtu.edu.cn

Received 5 January 2024; revised 15 March 2024; accepted 17 March 2024; posted 18 March 2024; published 16 April 2024

The development of fast, efficient, and cost-effective tunable optical filters is a tireless pursuit of the goal in the field of optical signal processing and communications. However, the traditional filters have been limited by their complex structures, slow tuning speed, and high cost. To address this challenge, we present a tunable ultra-narrow band-pass filter, which is fabricated by a metal layer cladded in a high-parallelism and high-precision piezoelectric ceramic for an interlayer. Experimental results show a remarkable full width at half maximum of 51 pm and a fast response time of 800 ns. In addition, by cascading double filters, the wavelength of the output light has been fine-tuned from a Vernier effect. Moreover, we realize a tunable filter to select and output several ultra-narrow single peaks with 56% efficiency in the 2 nm range. Furthermore, it offers a wide tunable range, exceptional narrowband filtering performance, and fast piezoelectric response times. Hence, it is particularly well suited to applications requiring precise wavelength selection and control, opening new possibilities in the field of tunable optical filters.

https://doi.org/10.1364/OL.517815

Recently, there has been a significant surge in the demand for highly selective and tunable optical filters in the field of photonics and communications. Herein, optical filters play a pivotal role in numerous applications, including telecommunications, spectroscopy, sensing, and imaging [1–5]. In optical communications, tunable waveguide filters play a crucial role in achieving wavelength division multiplexing and wavelength conversion within high-speed and adaptive optical signal processing systems [5–7]. In spectroscopy, tunable optical filters with high resolution and precise wavelength selection capabilities are essential for the separation and analysis of intricate spectral features. This holds immense significance in the analysis of absorption, emission, and scattering spectra [8]. For optical sensing and imaging, tunable filters facilitate the analysis and detection of light signals within specific wavelength ranges, enabling optical measurements and imaging with high resolution and high sensitivity [9–12]. With the development of technology, the demand for higher resolution spectroscopy, high-capacity optical communications, and high-precision optical sensing applications has become increasingly urgent. This has ushered in a new era of research and development in the field of optical filters.

Various methods are employed to achieve tunable filtering functionalities, including electro-optic tunable filters [13], acousto-optic tunable filters [14], birefringent tunable filters [15], liquid crystal (LC) tunable filters [16], and micro-electromechanical systems (MEMS) [15,17]. These methods often face limitations in practical applications, such as limited tuning ranges, lower resolution, and complex manufacturing processes. For instance, electro-optic tunable filters may require high driving voltages, leading to increased energy consumption and system complexity. Acousto-optic tunable filters typically exhibit bulky dimensions and relatively slow tuning speeds. Birefringent tunable filters demand elongated optical pathways and intricate device structures, often comprising multiple optical components such as birefringent crystals, wave plates, and polarizers, to achieve tunability. Meanwhile, the alignment and calibration of these components often demand meticulous adjustments and preparations, thereby escalating device complexity and manufacturing costs. LC devices represent a common approach for achieving a tunable filtering effect, relying on the adjustment of LC molecule orientations to modify light transmission properties. However, LC devices are characterized by limited tuning ranges and often exhibit slow response speed, hindering them from the applications requiring rapid tuning response. The MEMS technology is also employed in the field of filters, relying on the movement of minuscule mechanical structures to fine-tune filter characteristics. The manufacturing process is labor-intensive and faces challenges related to reliability and stability due to the intricate nature of MEMS structures. In addition, MEMS-based systems often have limited resolution, making them unsuitable for ultra-narrowband filtering requirements.

Moreover, with the development of waveguide technology, waveguides have emerged as a highly effective method for fabricating tunable optical filters [18,19], which can manipulate and control light transmission by adjusting their structure and material properties, enabling tunable filtering functionality.

According to the research results, waveguide-based tunable filters offer several advantages. Firstly, waveguide structures facilitate high integration and compactness, suitable for various optical devices and systems. Secondly, waveguide material and structural properties can be selectively tailored for tunability across diverse wavelength spectra. Furthermore, waveguide technology can be combined with other tuning mechanisms, such as piezoelectric ceramic transducers (PZT) [20] and LC [16], to further expand the tuning range and enhance overall performance.

The metal film waveguide (MFW) possesses numerous outstanding optical properties [21–26]. The most exceptional characteristic of MFW is the excitation of ultrahigh-order eigenmodes (UOMs) within the guided layer, making it an ideal candidate for ultra-narrow filters. MFW-based filters offer high tunability, broad operational wavelengths, and ease of fabrication and integration. The filtering is achieved through the exploitation of optical coupling and resonance within the waveguide layer, rendering it suitable for applications demanding high selectivity, tunability, and a broad wavelength range due to the properties of metal. The straightforward fabrication and integration characteristics establish it as an effective solution for producing high-performance tunable filters in photonics. Owing to these attributes, we propose a unique design that utilizes the precise thickness control capabilities of PZT to modulate the waveguide cavity's thickness, which combines the MFW with a high-parallelism and high-precision PZT driver, resulting in a tunable ultra-narrow bandpass filter named as the symmetrical Ag film cladding PZT waveguide (SAPW). PZT, under external voltage control, can achieve rapid and precise thickness adjustments of MFW, which offers high reliability, stability, and wide tuning range. Furthermore, both PZT and the planar waveguide structure are suitable for integration, enabling compact device designs for application. The design features a guided layer consisting of PZT and BK7 plate glass, flanked by metal cladding layers, constituting a resonant layer that efficiently traps light within the waveguide. Precise wavelength tuning and mode selection around 1064 nm were accomplished through the precise control of the waveguide layer's thickness using PZT. In addition, we realize an ultra-narrowband filter with a full width at half maximum (FWHM) of 51 pm, a modulation speed of 800 ns, and an efficiency of 56% by using the Vernier effect with two SAPWs. The ultra-narrow tunable filter offers new opportunities for high-resolution spectroscopy, optical communications, and sensing applications.

The MFW is a three-layer structure, consisting of two Ag film layers and the guided layer, as shown in Fig. 1(a). Compared with the traditional dielectric waveguide, the MFW possessed fascinating properties, the ability of free-space coupling and UOMs (see more details in Supplement 1, Section I). Figure 1(b) shows the dispersion curve of the waveguide and illustrates a relationship between the thickness of the guiding layer and the transmission mode, indicating the potential for the design of tunable filter. As shown in Fig. 1(c), the attenuated total reflection (ATR) of the incident laser with different propagation constants from air is characterized with several coupling peaks. For the incident angle of the laser reaching the resonance condition (the propagation constant of the incident light in the propagated direction is in resonance with the eigenstates of the MFW), it will be coupled into the MFW due to the free-electron resonance effect of the upper Ag film and then transmitted through the waveguide by the free-electron resonance effect of the thin Ag

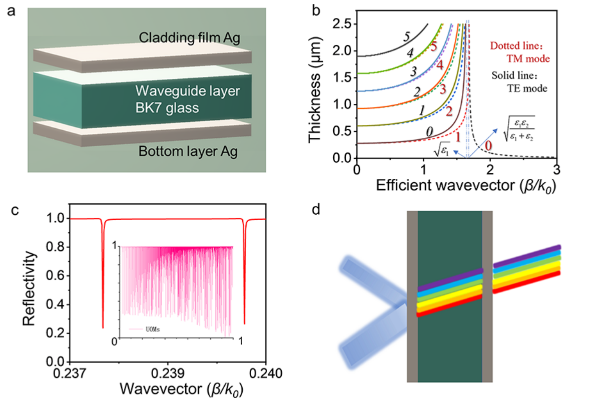

Fig. 1. (a) Diagram of the MFW consisting of two Ag films and BK7. (b) Dispersion equation of MFW. (c) Simulation of the relationship between reflectivity and wave vector. (d) Scheme of the filter effect of MFW.

film, while the incident laser without resonance condition will be totally reflected. Moreover, for the wideband laser with the same incident angle, the propagation constants will be different among various wavelengths, indicating that the transmission spectrum will be discrete and become an optical comb (see more details in Supplement 1, Section I). As a result, by using a MFW, the wideband laser is filtered as depicted in Fig. 1(d). When the broadband incident light (broadband blue light) is incident on the MFW, it experiences wavelength-selective effects within the waveguide. As a result, a portion of the light that cannot be coupled into the waveguide is reflected (narrower blue light).

For practical application integration, we adopt the transmission mode of the MFW with thin silver films on both the top and bottom surfaces. As shown in Fig. 2(a), the symmetrical Ag film cladding PZT waveguide (SAPW) and the inset show the two SAPWs used in the experiments. To avoid the photoelectric effect of PZT, we design the main structure as a ring-shaped hollow PZT with the air layer as the guided layer. The PZT surfaces were polished, optically bonded with glass for parallelism under 4″, and metalized with a uniform Ag film via evaporation coating. The inner layer is an Ag film of uniform thickness, with an outer Au film serving as a protective layer. Figure 2(b) shows the coupling efficiency of the two SAPWs under 1064 wavelength laser irradiation (both SAPW structures have sufficiently high coupling efficiencies of 91.5% and 93.6%, respectively). Figure 2(c) shows the schematic diagram of the experimental optical setup where the filtering effect of the SAPW is used to achieve the filtering of the broadband laser beam emitted by the amplified spontaneous emission (ASE) source. A collimated beam from an ASE light source (1000–1100 nm) is directed at a shallow angle onto the SAPW using free-space coupling. The transmitted signal is analyzed by a spectrometer to assess the SAPW's filtering performance. Figure 3(a) shows the theoretical transmission spectrum of the incident light through a 1 mm waveguide layer with a central wavelength of 1064 nm at an incidence angle of 0.1 pai, with a narrowband filtered FWHM of around 2.8 pm. In the experiment we used two thicknesses of PZT, D1 (0.83 mm) and D2 (1.07 mm), which are suitable for single mode filtering in terms of the density of the UOMs. We measured the transmission spectra of the two SAPWs, as shown in Figs. 3(b) and 3(c). After filtering the broadband laser by a single SAPW, the resulting output signal indeed resembles an

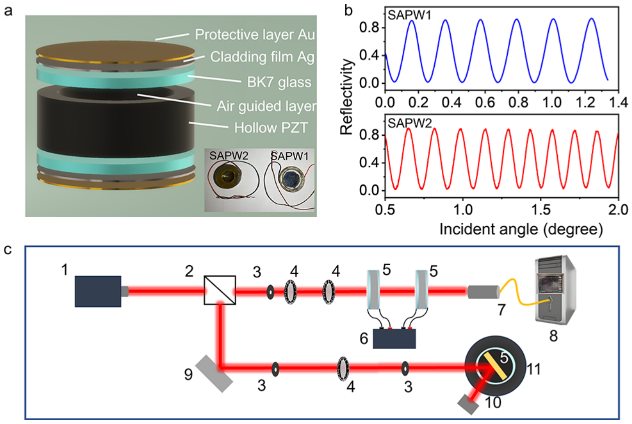

Fig. 2. (a) Diagram of the SAPW and photo of real structures. (b) Experimental data for the detected ATR of two SAPWs. (c) Optical experimental setup. 1. laser source, 2. polarization beam splitter (PBS), 3. spot, 4. polarizer, 5. SAPW, 6. direct-current power, 7. optical fiber probe, 8. spectrum analyzer, 9. reflector, 10. photonic detector (PD), 11. $\theta/2\theta$ synchronous rotator.

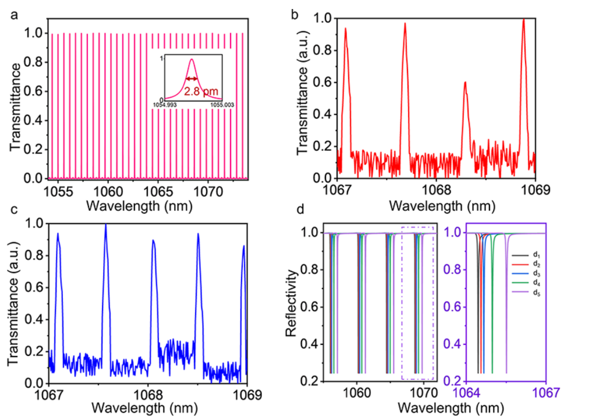

Fig. 3. (a) Theoretical transmitted spectrum of the SAPW. (b), (c) experimental transmitted spectra of the SAPW1 and SAPW2, respectively. (d) Shift of the transmitted spectrum of the SAPW with different thicknesses (d = 1 mm, d1 = d + 0.01 μm, d2 = d + 0.02 μm, d3 = d + 0.05 μm, d4 = d + 0.1 μm) guided layers.

optical comb in accordance with theoretical expectations. It is noteworthy that a thicker waveguide layer leads to a higher mode density, which is supported by the theory.

As mentioned above, waveguide modes are sensitive to changes in thickness. Figure 3(d) illustrates that the modes shift within a narrow range when the thickness is varied. Therefore, adjusting the thickness of the SAPW can change the mode distribution (as detailed in the Supplement 1, Section II). A single SAPW generates a comb spectrum, hindering the attainment of a pure single peak. Employing the Vernier effect through the cascade of two distinct-mode SAPWs enables an ultra-narrowband single peak filter. (See Fig. 4(a)). Moreover, the coupling peak can shift proportionally to the thickness of the guided layer in a small range. For the MFW, the reduced dispersion equation can be obtained as

$$\kappa_2 h = m\pi, \tag{1}$$

where, $\kappa_2 = ({k_0}^2\varepsilon_2 - \beta^2)^{1/2}$, k_0 is the wave vector in vacuum, ε_2, is the relative dielectric constant of the cladding film, $\beta =$

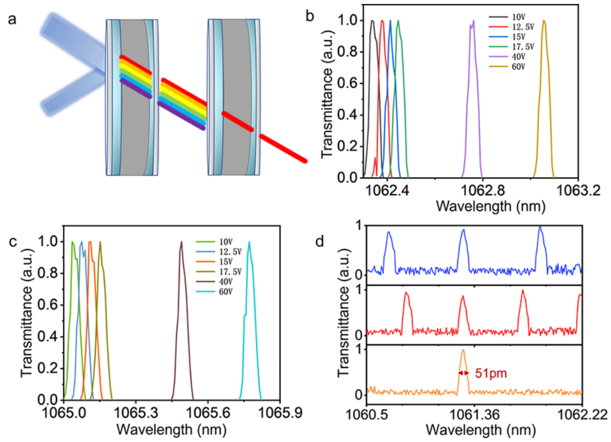

Fig. 4. (a) Single transmitted peak realized by cascaded SAPWs. (b), (c) shift of a single peak with different loaded voltages for SAPW1 and SAPW2, respectively. (d) Single transmitted peak with cascaded SAPWs.

$k_0\sqrt{\varepsilon}\sin(\theta)$ is the propagation constant, θ is the incident angle in air, and h is the thickness of the guided layer. Therefore, by changing h, the resonant lambda of the m-order eigenmode becomes

$$\Delta\lambda = -\frac{2{\kappa^2}_2}{h({k_0}^2\frac{2}{\lambda}(\sin^2(\theta) - \varepsilon_2) + {k_0}^2\alpha)}\Delta h, \tag{2}$$

where $\alpha = \partial\varepsilon_2/\partial\lambda$ is the first derivative of the dielectric constant of the cladding film with respect to the lambda. Therefore, we can proportionally modify the coupling wavelength by changing the loaded voltage.

The experimental spectrum shows the peak modulation in response to the PZT voltage for two SAPWs (Figs. 4(b) and 4(c)). As the applied voltage varies, the thickness and the transmission mode of the waveguide also change as mentioned in Fig. 1(b), so its resonance wavelength also changes accordingly. In other words, adjusting the PZT voltage tunes the transmission wavelengths of the two SAPWs individually, facilitating single mode peak filtering via their Vernier effect. We achieve ultra-narrowband filtering at 1061.27 nm with a FWHM of 51 pm (Fig. 4(d)). The top area shows the transmission spectrum of SAPW1 at 15.25 V, the middle area shows the transmission spectrum of SAPW2 at 31.63 V, and the bottom area shows

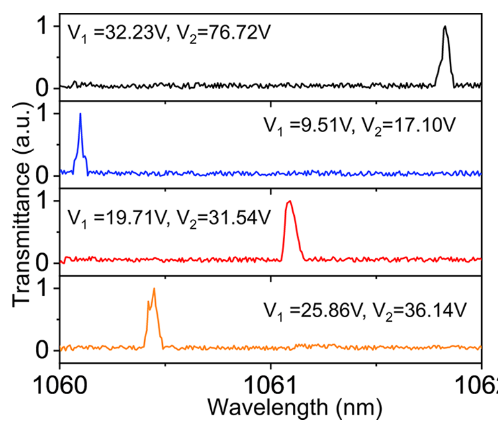

Fig. 5. Demonstration of several ultra-narrow spectra based on cascaded SAPWs with various loaded voltages.

Table 1. Comparison of Other Quickly Tunable Filters

Num.	Full Width at Half Maximum	Speed	Wavelength Adjustable Range	Physical Mechanism
1 (ours)	0.051 nm	800 ns	2 nm	SAPW
2 [27]	0.47 nm	——	0.34 nm	Microring based on silicon
3 [28]	≈5 nm	500 ns	6 nm	PMN-PT Fabry–Perot cavity
4 [29]	≈2 nm	1 ms	5.6 nm	MEMS silicon waveguide
5 [14]	>1 nm	——	450 nm	Acousto-optic
6 [30]	4 nm	≈1 ms	400 nm	Liquid crystal Fabry–Perot cavity

the ultra-narrowband spectrum obtained by the Vernier effect of the two cascaded SAPWs. We also conducted repeatability and stability tests; details are provided in Supplement 1, Figs. S4 and S5. To demonstrate the flexible ultra-narrow filtering of our cascaded SAPW system, we achieved multiple ultra-narrowband spectra from 1060 to 1062 nm by tuning the voltages of the two SAPWs, as depicted in Fig. 5.

In conclusion, we propose a quickly tunable ultra-narrowband filter based on a MFW structure and an accurate PZT driver, referred to as SAPW. As shown in Table 1, compared to other quickly tunable filters, the proposed filter has an exceptional narrowband filtering capability and rapid piezoelectric responsivity, making it ideal for applications that require precise wavelength selection and tuning. In practical applications, temperature variations and mechanical vibrations can influence the performance of SAPW devices. To minimize these effects, a temperature-controlled system can be employed, and closed-loop control can be implemented to mitigate the impact of mechanical vibrations induced by PZT elements. We believe that the demonstrated filter performance will play an important role in the advancement in optics and photonics, providing new options for high-resolution spectroscopy, optical transmission, optical measurement, optical imaging and other fields.

Funding. Natural Science Foundation of Shanghai (23ZR1428400); Shanghai Municipal Science and Technology Major Project (2019SHZDZX01-06); National Natural Science Foundation of China (12104298, 12192252).

Acknowledgment. Thanks for the support from the Laboratory of Advanced Photonic Materials and Physics, Shanghai Jiao Tong University.

Disclosures. The authors declare no conflicts of interest.

Data availability. Data underlying the results presented in this paper are not publicly available at this time but may be obtained from the authors upon reasonable request.

Supplemental document. See Supplement 1 for supporting content.

REFERENCES

1. H. Herrmann and K. Schafer, IEEE Photonics Technol. Lett. **10**, 120 (1998).
2. E. L. Wooten, R. L. Stone, E. W. Miles, *et al.*, J. Lightwave Technol. **14**, 2530 (1996).
3. C. K. Madsen, J. A. Walker, J. E. Ford, *et al.*, IEEE Photonics Technol. Lett. **12**, 651 (2000).
4. K. Hirabayashi and H. Tsuda, IEEE Photonics Technol. Lett. **3**, 213 (1991).
5. J. S. Patel, M. A. Saifi, D. W. Berreman, *et al.*, Appl. Phys. Lett. **57**, 1718 (1990).
6. E. C. Silva-Alvarado, A. Martinez-Rios, E. Gallegos-Arellano, *et al.*, Opt. Laser Technol. **149**, 107824 (2022).
7. Y. F. Lu and Y. C. Lin, IEEE Trans. Antennas Propagat. **61**, 5395 (2013).
8. H. Grün, T. Berer, P. Burgholzer, *et al.*, J. Biomed. Opt. **15**, 021306 (2010).
9. J. Xia, F. Wang, H. Luo, *et al.*, Sensors **16**, 620 (2016).
10. C. Lin, H. Luo, S. Xiong, *et al.*, Proc. SPIE **9297**, 929735 (2014).
11. M. A. Bolshov, Y. A. Kuritsyn, and Y. V. Romanovskii, Spectrochim. Acta, Part B **106**, 45 (2015).
12. N. D. Lourenço, J. A. Lopes, C. F. Almeida, *et al.*, Anal. Bioanal. Chem. **404**, 1211 (2012).
13. R. Kim, J. Zhang, O. Eknoyan, *et al.*, Electron. Lett. **41**, 1220 (2005).
14. V. I. Batshev, A. S. Machikhin, A. B. Kozlov, *et al.*, J. Commun. Technol. Electron. **65**, 800 (2020).
15. M. Meinig, M. Ebermann, N. Neumann, *et al.*, in *International Conference on Solid-State Sensors, Actuators and Microsystems* (2011), p. 2538.
16. P.-L. Chen, K.-C. Lin, W.-C. Chuang, *et al.*, IEEE Photonics Technol. Lett. **9**, 467 (1997).
17. H. Mao, K. K. M. B. D. Silva, M. Martyniuk, *et al.*, J. Microelectromech. Syst. **25**, 227 (2016).
18. Z. Wang, F. Wei, L. Zhang, *et al.*, Prog. Electromagn. Res. Lett. **41**, 193 (2013).
19. H. Lu, X. Liu, D. Mao, *et al.*, Opt. Express **18**, 17922 (2010).
20. G. L. Smith, J. S. Pulskamp, L. M. Sanchez, *et al.*, J. Am. Ceram. Soc. **95**, 1777 (2012).
21. H. Li, Z. Cao, H. Lu, *et al.*, Appl. Phys. Lett. **83**, 2757 (2003).
22. Y. Wang, Z. Cao, T. Yu, *et al.*, Opt. Lett. **33**, 1276 (2008).
23. H. Dai, C. Yin, X. Ye, *et al.*, Sci. Rep. **7**, 3174 (2017).
24. H.-L. Dai, C. Yin, Z.-y. Xiao, *et al.*, Phys. Rev. Appl. **11**, 064055 (2019).
25. H. Dai, L. Yuan, C. Yin, *et al.*, Phys. Rev. Lett. **124**, 053902 (2020).
26. Q. Wei, H. Dai, H. Shan, *et al.*, Phys. Rev. B **104**, 235308 (2021).
27. L. Liu, W. Xue, X. Jin, *et al.*, IEEE Photonics J. **11**, 1 (2019).
28. H. Jiang, Y. K. Zou, Q. Chen, *et al.*, in *Optoelectronic Devices & Integration* (2005).
29. C. Bolle, A. Sridhar, H. Safar, *et al.*, IEEE Photonics Technol. Lett. **30**, 837 (2018).
30. Z. Zheng, G. Yang, H. Li, *et al.*, Opt. Express **19**, 2158 (2011).